Journal of Alloys and Compounds 509 (2011) 6497–6501

Contents lists available at ScienceDirect

Journal of Alloys and Compounds

journal homepage: www.elsevier.com/locate/jallcom

In situ infrared thermographic screening of compositional spread Mg–Ti thin-film libraries

Roger Domènech-Ferrer[a], Javier Rodríguez-Viejo[a,b], Marta González-Silveira[a], Gemma Garcia[a,*]

[a] Group of Nanomaterials and Microsystems – GNaM, Physics Department Universitat Autònoma de Barcelona, Campus UAB – Torre C3-222, 08193 Bellaterra, Spain
[b] MATGAS Research Centre, Campus UAB, 08193 Bellaterra, Spain

ARTICLE INFO

Article history:
Received 22 December 2010
Received in revised form 17 March 2011
Accepted 18 March 2011
Available online 29 March 2011

Keywords:
Infrared thermography
MgTi
Hydrogen storage
Combinatorial or high throughput
Thin films
Kinetic analysis

ABSTRACT

An infrared imaging set-up and our own data treatment methodology have been developed to investigate hydrogen storage properties of combinatorial metallic thin-film libraries in situ. The technique has been tested by analysing the kinetics of hydrogen sorption and desorption in pure metallic magnesium films and in compositional-spread Mg–Ti libraries. Thermography was used to screen the surface emissivity of the libraries, since hydrogenated and dehydrogenated phases present very different values of this property. The proposed data treatment allows for direct visualisation of onset reaction temperatures ($T_{hydrogenation}$ and $T_{dehydrogenation}$) in function of composition which, in the present case, clearly reveals the catalytic influence of titanium on the kinetic properties of magnesium film dehydrogenation.

1. Introduction

One of the main drawbacks for moving towards a clean hydrogen energy economy is the lack of efficient, safe hydrogen storage technology. Nowadays, solid state storage is seen as one of the possible alternatives to high pressure gas tanks, which are considered to have safety concerns. Solid hydrides presenting high volumetric and gravimetric densities are needed to provide all the technical and economic requirements for the real development and implantation of such technology. In order to speed up efforts to find lightweight metal and complex hydrides as promising storage materials, a great deal of work has been done in recent years to develop combinatorial synthesis and high-throughput screening methodologies, mainly based on the thin-film approach [1–11].

Unfortunately, standard characterization methods of gas/solid interactions in bulk samples, such as volumetric (e.g. Sieverts) and gravimetric (e.g. thermogravimetric analysis – TGA) techniques, cannot be used in such low-volume systems. The development of in situ screening techniques for spatially controlled or compositionally graded thin-film libraries has become a key factor for the success of the combinatorial approach. Optical methods have recently been confirmed as powerful techniques due to their apparent simplicity and low cost. In 1996, Huiberts et al. [12] observed real-time transition from metallic to semiconducting states during hydrogen absorption in several thin films. Since then, the large optical property changes observed during hydrogenation of thin films have been used in a large number of high-throughput screening applications such as catalysts for hydrogen production [13], localised hydrogen sensors using optical fibres [14], switchable mirrors [15,16] and solar cell collectors [17,18]. Based on these optical reflective changes, Griessen et al. developed the hydrogenography technique [3,5] which allows the simultaneous determination of hydrogenation enthalpies of thousand-alloy compositions [4,19], thus enabling the combinatorial study of thermodynamics and kinetics of novel hydrogen storage alloys. While hydrogenography is based on optical transmission/reflection variations during hydrogenation, the infrared (IR) imaging initially proposed by Olk et al. [1,2] detects changes in emissivity. In conventional bulk samples hydrogenation and dehydrogenation reactions are also accompanied by changes in temperature, due to large reaction enthalpies (ΔH), which can be detected by thermography. Nevertheless, in the case of thin films, especially when deposited on highly conducting substrates such as silicon or sapphire, the temperature variation induced by the energetics of the transformation is much lower than the apparent temperature shifts due to surface emissivity variations, thus making screening of emissivity changes a more effective and precise methodology. Successful infrared screening of in situ alloy hydrogenation has already been reported by Olk et al. [1,2] in the multicompositional Mg–Ni–Fe system, more recently by Guerin et al. [7] and Oguchi et al. [8,9] in

* Corresponding author. Tel.: +34 935811481; fax: +34 935812155.
E-mail address: gemma.garcia@uab.cat (G. Garcia).

0925-8388/$ – see front matter © 2011 Elsevier B.V. All rights reserved.
doi:10.1016/j.jallcom.2011.03.118

the Mg–Ni system, and by our group in the Mg–Al and Mg–Fe–Cu systems [11]. Apart from the studies where the effect of alloy composition and microstructure on the hydrogenation properties have been thoroughly analysed, other studies have also recently demonstrated the use of IR imaging to characterise heterogeneous growth processes of the hydride phase on solid-state hydrogen storage materials such as Mg–Ti [20] and solving multiple phase transitions that can be found during hydrogen cycling, as in the case of yttrium film [21].

This paper describes the optimisation of infrared thermography as a time-resolved monitoring tool for analysis of the hydriding/dehydriding kinetic properties of a magnesium–titanium combinatorial thin-film library. A specific data treatment, enabling rapid screening of the hydrogen sorbing and desorbing temperatures during heating ramps as a function of the library composition, has been developed in order to generate reaction temperature maps which could directly identify superior hydride or hydride-promoter combination formulations. The Mg–Ti system was chosen due to the fast hydrogen reaction kinetics demonstrated in bulk [22] as well as in thin films [23–25].

2. Experimental

2.1. Infrared screening technique

The principle of infrared thermography is based on the physical phenomenon that any body at a temperature above absolute zero emits electromagnetic radiation. By determining its radiation power (W), the temperature of an object can thereby be determined in a non-contact way using the Stefan–Boltzmann law Eq. (1):

$$W = \sigma\varepsilon T^4 \quad (1)$$

The radiated power is thus proportional to the fourth power of the temperature and varies linearly with the emissivity (ε), where the **Stefan–Boltzmann constant** $\sigma = 5.7 \times 10^{-8}\ \mathrm{W\,m^{-2}\,K^{-4}}$. In addition, in the mid-to-far infrared range, the Hagen–Rubens relation Eq. (2) can be applied, which links the emissivity of a body with its resistivity:

$$\varepsilon = 2(2\varepsilon_0\omega\rho)^{1/2} \quad (2)$$

where ε_0 is the vacuum dielectric constant, ω is the angular frequency of the electromagnetic wave and ρ is the resistivity of the material. From this equation, we can conclude that insulators or semiconductors will generally have higher emissivities than metals. Consequently, as metal hydrides usually present higher resistivities than their corresponding pure metals, emissivity analysis can be successfully applied to monitor their hydrogenation and dehydrogenation.

Since infrared imaging is a non-contact procedure, the radiation travels over a certain distance and through several media before reaching the detector. Actually, a large part of the radiation emitted by the sample is partially reflected by the IR camera lenses and is partially reabsorbed either by the atmosphere either inside or outside the experimental chamber or by the screening window. Thus, the effective measured radiation (W'), is automatically converted via the camera software into an apparent temperature (T_a) defined as:

$$T_a = \left(\frac{W'}{\sigma}\right)^{1/4} = T(\varepsilon)^{1/4} \quad (3)$$

Any change in the measured T_a will be directly related to variations in sample emissivity and thus will be used to detect hydrogenation or dehydrogenation reactions in combinatorial samples.

2.2. Hydrogenation chamber

Hydrogenation treatments and in situ thermographic characterisations are performed in a chamber where pressure can vary from high vacuum to 1 bar of pure or mixed He and H_2 atmosphere and from room temperature to 300 °C (Fig. 1). An infrared camera, Jenoptik IR-TCM 384, was mounted above a ZnSe chamber viewport to record the sample IR images (388 × 284 data point/image) during thermal treatments. Before the experiments, the main chamber was purged with helium three times to minimize the presence of oxygen and moisture. IR image acquisition and thermal treatments were lumped together to assign a temperature/time correspondence during constant heating and isothermal treatments. Irbis 3.0 software provided by JENOPTIK allows visualization and basic feature analysis of IR images such as determination of the single point apparent temperature, average temperature over a selected surface and temperature profiles of any path.

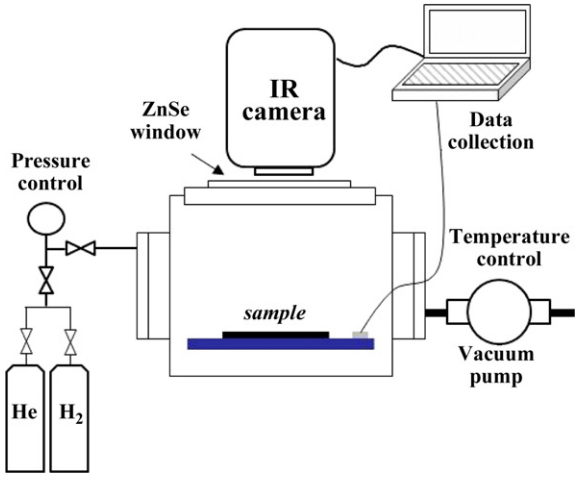

Fig. 1. Scheme of the infrared thermography experimental set-up.

2.3. Preparation of thin-film magnesium–titanium libraries

The Mg–Ti libraries were prepared on 3 cm × 3 cm Si substrates using DC sputtering in the co-deposition compositional-graded approach. The combinatorial growth is based on the natural thickness gradient ensured by an off-axis tilting of the metallic target guns and non-rotation of the substrate. Mg (200 W) and Ti (150 W) were co-evaporated simultaneously at 2×10^{-2} mbar of Ar, to obtain a mixture of Mg and Ti which produced a library with a thickness of 130 ± 20 nm. Finally, the library was capped with a uniform 10 nm Pd (25 W) layer. All films were deposited at room temperature. The palladium cap layer was added to catalyse the hydrogen molecule dissociation, thus improving the kinetic properties of the magnesium and drastically reducing the absorption and desorption temperatures even to room temperature [14,26–29]. The composition of the library was estimated by energy dispersive X-ray spectroscopy over 16 points distributed across the sample forming a 4 × 4 matrix.

3. Results and discussion

3.1. Thermography optimization

The feasibility of the experimental setup was first checked by characterising simple systems such as metallic Cu and Mg thin films (210 nm) and then comparing their behaviour with that of a semiconducting sample, i.e. silicon wafer. A cap layer of 10 nm Pd was used on top of magnesium to ensure atomic hydrogen diffusion while avoiding any further oxidation. To simulate identical surface conditions, the copper layer was also coated with 10 nm of palladium. The experiment consisted of heating up the samples in helium (1 bar) at 10 °C/min up to 150 °C, consecutively introducing pure hydrogen in the chamber for 1 h, cooling down the sample to ambient temperature, followed by a heating ramp up to 250 °C in helium at 10 °C/min. These experimental parameters (temperatures, pressure, gases) were selected in order to check the conditions that will be used in further analyses to perform hydrogenation and dehydrogenation reactions. Fig. 2 shows the IR thermographs acquired for the three representative samples at different times of the whole treatment: (a) at 150 °C in 1 bar He; (b) after 1 h of treatment at 150 °C in 1 bar H_2, and (c) after helium annealing at 215 °C. As clearly seen in Fig. 1 the samples show a different, but uniform, apparent temperature over their entire surface.

At 150 °C in He (Fig. 2a), both metallic copper and magnesium films present a similar apparent temperature, but it is lower than that of the semiconducting Si substrate, in agreement with the Hagen–Rubens law. On the other hand, when samples are annealed in hydrogen (Fig. 2b) only Mg film emissivity, and thus its T_a, changes due to the formation of semiconducting MgH_2 hydride. As expected, neither the Cu film nor the silicon absorbs hydrogen under the studied experimental conditions and their apparent

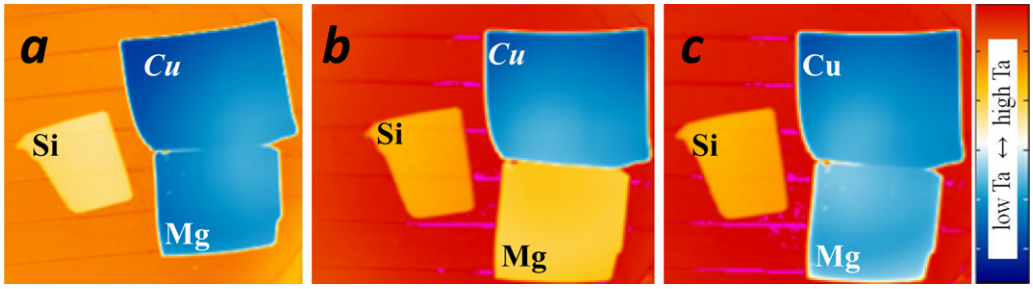

Fig. 2. Thermal images of silicon substrate, and Cu and Mg thin films coated with 10 nm of Pd; (a) at 150 °C in He, (b) after 1 h at 150 °C in H_2 – hydrogenation conditions and (c) after heated at 215 °C in He – after dehydrogenation treatment. (For interpretation of the references to color in this figure legend, the reader is referred to the web version of the article.)

temperatures remain unchanged. Fig. 2c shows the thermograph captured during the heating ramp up to 250 °C in helium, which was done in order to force dehydrogenation. As seen in the image acquired at 215 °C, the magnesium sample recovers its initial apparent temperature thus confirming the fact that the dehydrogenation process has taken place by transforming the former hydride into a metallic Mg film. Note that the experimental parameters of the three selected thermographs correspond to three representative states: the initial-metallic, hydrogenated-semiconducting and final-metallic state of the magnesium sample and not to any transition condition threshold. The previous experiment also confirms the negligible effect of thin Pd films (10 nm) on emissivity changes arising from the formation of the PdH_x compound, as was expected from the work of Oguchi et al. [8], which sets the critical blocking thickness at 30 nm.

Although information can be directly extracted from a single image, the determination of exact reaction temperatures as a function of time, and/or sample composition, especially in combinatorial libraries, requires detailed data analysis. To this end, image sequences were acquired at 10 images per minute and each of them was transformed into an ASCII format matrix of 388 × 284 pixels. Each pixel corresponded to the apparent temperature at a particular point of the sample surface and thus to a precise sample composition. Matlab® routines were developed to mathematically analyse the evolution of apparent temperature with temperature for each matrix pixel allowing for the extraction of the de/hydrogenation temperature onsets.

An example of the T_a change during a heating ramp, in order to produce dehydrogenation, is shown in Fig. 3. In this case, we heated up a 210 nm thick magnesium film coated with 10 nm palladium at 10 °C/min at two different hydrogen partial pressures, 10 and 100 mbar. The Mg samples were previously hydrogenated in 1 bar of H_2 at 100 °C for 1 h and cooled down to room temperature. T_a increases monotonously with temperature following the heating ramp until a temperature where the semiconducting MgH_2 transforms into pure metallic Mg and T_a decreases abruptly. After hydrogen desorption, the apparent temperature of the samples increases again due to the temperature ramp. Furthermore, as expected, desorption at lower partial pressure (10 mbar) takes place at a lower temperature (around 145 °C) than at higher pressure (P_{H_2} = 100 mbar), which occurs at about 175 °C.

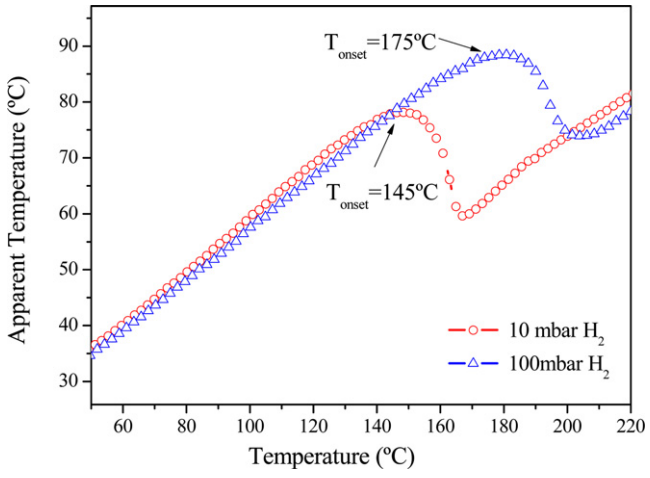

Fig. 3. Apparent temperature of 210 nm Mg coated with 10 nm Pd in 10 and 100 mbar of pure hydrogen versus temperature (heating rate of 10 °C/min).

The determination of onset reaction temperatures by defining the T_a slope deviation point in heating ramp procedures is not always easy and complementary data treatment is needed to accurately determine the transition values. To this end, we have developed and applied the so-called differential data treatment to all measurements. The apparent temperature of the metallic heater surface (T_H) is simultaneously acquired and subtracted from the sample apparent temperature (T_a). The stainless steel metallic heater presents low emissivity, typical of metals, and is not expected to react within the studied range of temperatures and hydrogen partial pressure. Its apparent temperature (T_H) evolution can thus be used as a background reference. This data analysis methodology allows discriminating T_a changes produced by heating or cooling from those really corresponding to any hydride formation or decomposition as well as to any other chemical reaction that produces a variation in emissivity.

3.2. Mg–Ti thin-film library characterisation

Interpolation of EDS content values using a second-order polynomial enables evaluation of the total surface composition map shown in Fig. 4. The magnesium gradient almost follows a linear trend from one side of the library to the other. The gradient varies from 98 at.% to 69 at.% The corresponding titanium compositional gradient shows an opposing trend as it changes from 2 to 31 at.%.

Infrared imaging was then used to monitor the dehydrogenation process of the library that was previously in situ hydrogenated in 1 bar of pure H_2 for 60 min at 100 °C. Dehydrogenation was performed by heating up the sample to 170 °C in pure helium at a rate of 10 °C/min. Kinetic analysis is limited to the dehydrogenation process as almost all the complete library hydrogenated instantaneously at room temperature after hydrogen was introduced into the chamber. Changes in emissivity to hydrogenated values were so rapid, compared with the camera acquisition time, that we were unable to analyse the hydrogenation process. Visual inspection of the thermograph sequences gives a general trend of the effect of titanium content on desorption temperatures, as shown in Fig. 5, which shows four instants of the heating sequence.

As seen in Fig. 5, the whole surface of the library shows a uniform T_a, at lower temperature, with a clear colour corresponding

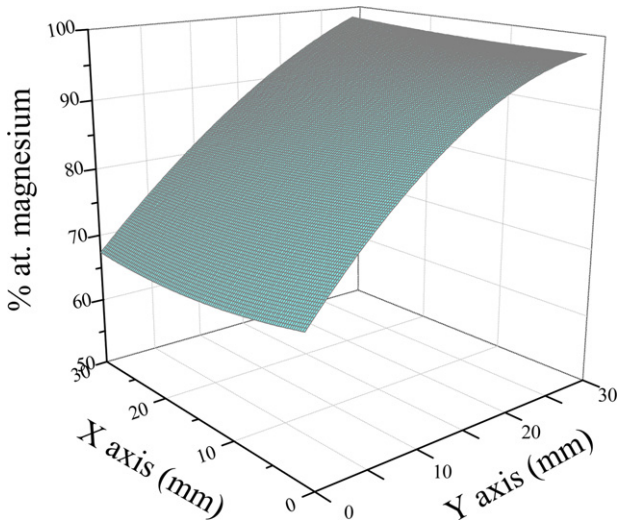

Fig. 4. Interpolated Mg–Ti compositional graded map over the 3 cm × 3 cm sample surface in % atomic of magnesium.

to the hydrogenated state. When the temperature is increased, the emissivity changes from the semiconductor state – clearer zones (hydrogenated) to the metallic state – darker zones (dehydrogenated) states. As the library was placed in such a way that the titanium-rich part is found in the upper part of the images, we clearly see that hydrogen desorption, i.e. the transition from clear to dark images, starts in the upper Ti-rich area of the sample. As the temperature increases, the dark areas spread to the lower part of the sample which reaches an almost uniform dark aspect that corresponds to complete dehydrogenation.

Applying the data treatment procedure described above to the image sequences, we have constructed an onset dehydrogenation temperature map (Fig. 6a), where image data is converted into usable values. This illustrates the ability of infrared thermography for high-throughput characterisation of metal hydride libraries. In this map, we have assigned a desorption onset temperature to any point of the compositional library surface. If we then compare the dehydrogenation map with the compositional map, we can confirm what was already expected from the thermal image sequences, i.e. the dehydrogenation temperature clearly decreases with increase of Ti content, as has been described in the literature [29–34].

An exact direct relation between dehydrogenation temperature and titanium content is extracted by merging the two data maps (Fig. 6b). Clearly for Mg–Ti alloys in the measured range, i.e. with titanium ranging from 2 to 31 at.%, the dehydrogenation temperature decreases as the titanium content increases from 143 °C ± 3 °C to 94 °C ± 3 °C which confirms its catalytic effect on desorption. These values agree quite well with dehydrogenation onset temperatures measured by our group using nanocalorimetry [25] on discrete compositions, $T_{dehydro} \approx 140$ °C for pure magnesium film (200 nm) and $T_{dehydro} \approx$ around 90 °C for $Mg_{80}Ti_{20}$ film (200 nm). The error bar shown in Fig. 6b is defined by averaging the onset temperature along the *X* axis i.e. along almost-uniform magnesium

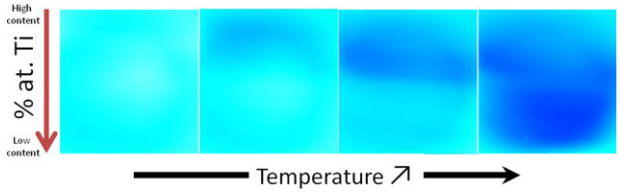

Fig. 5. IR images evolution during annealing in 1 bar of He at 10 °C/min. Clear zones correspond to low T_a, while dark areas correspond to dark zone high T_a.

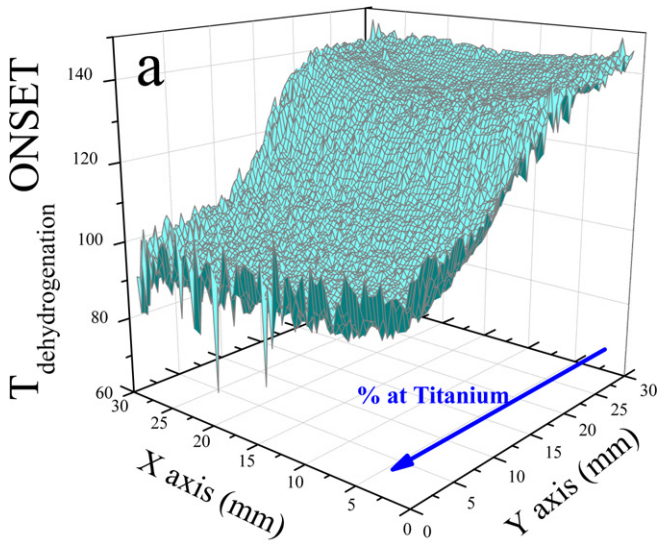

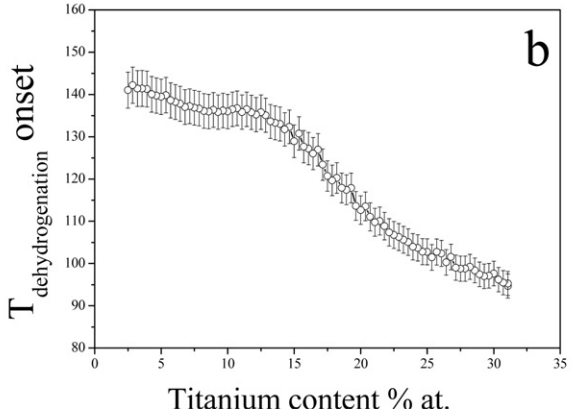

Fig. 6. (a) $T_{dehydrogenation}$ map for the dehydrogenation and (b) variation of $T_{dehydrogenation}$ as a function of titanium content.

compositions. This representation highlights the fact that desorption temperature decreases at different rates in function of titanium content. Two zones can be clearly defined, from 2 to ~10 at.% where the variation of the hydrogen desorption temperature in function of titanium content only decreases by 5 °C, i.e. 3.5%, and a region from 12 to 31 at.%, where the desorption temperature drops more than 40 °C (≈30%).

Although it is tempting to relate those two desorption behaviours to the two hydride phases observed by other authors [29–34]: a centred tetragonal structure for Ti < 10 at.% and a face cubic-centred structure for large Ti > 12 at.%, which is claimed to be responsible for the difference in the transport properties observed in function of titanium content, further characterization of our libraries is needed to confirm this probable hypothesis.

4. Conclusions

We have both prepared and characterized MgTi combinatorial libraries using the co-sputtering technique. IR thermography was successfully applied as a high-throughput technique to characterise the hydrogen desorption kinetics in this composition-graded library. The developed data processing routines enabled the determination of dehydrogenation temperature maps for each composition/pixel of the library. By previously determining the composition map of the sample, we were able to match both maps and assign a $T_{dehydrogenation}$ to titanium content. We have thus cor-

roborated the kinetic effect of titanium in the hydrogen desorption of magnesium hydride thin films. Although the proposed technique does not allow for direct quantification of the formed hydride, it is a valuable tool for fast identification of reaction promoters and for any kinetic characterisation in general.

References

[1] C.H. Olk, G.G. Tibbetts, D. Simon, J.J. Moleski, J. Appl. Phys. 94 (1) (2003) 720–725.
[2] C.H. Olk, Meas. Sci. Technol. 16 (2005) 14–20.
[3] R. Gremaud, A. Borgschulte, C. Chacon, J.L.M. van Mechelen, H. Schreuders, A. Züttel, B. Hjörvarsson, B. Dam, R. Griessen, Appl. Phys. A 84 (2006) 77–85.
[4] B. Dam, R. Gremaud, C. Broedersz, R. Griessen, Scripta Materialia 56 (10) (2007) 853–858.
[5] R. Gremaud, C.P. Broedersz, D.M. Borsa, A. Borgschulte, P. Mauron, H. Schreuders, J.H. Rector, B. Dam, R. Griessen, Adv. Mater. 19 (19) (2007) 2813.
[6] G. Garcia, R. Domènech-Ferrer, F. Pi, J. Santiso, J. Rodríguez-Viejo, J. Comb. Chem. 9 (2007) 230–236.
[7] S. Guerin, B.E. Hayden, D.C.A. Smith, J. Comb. Chem. 10 (2008) 37–43.
[8] H. Oguchi, J. Hattrick-Simpers, I. Takeuchi, E.J. Heilweil, L.A. Bendresky, Rev. Sci. Instrum. 80 (2009) 073707.
[9] H. Oguchi, E.J. Heilweil, D. Josell, L.A. Bendersky, J. Alloys Compd. 477 (1–2) (2009) 8–15.
[10] R. Gremaud, J.L.M. van Mechelen, H. Schreuders, M. Slaman, B. Dam, R. Griessen, Int. J. Hydrogen Energy 34 (2009) 8951–8957.
[11] R. Domènech-Ferrer, J. Rodríguez-Viejo, G. Garcia, Catal. Today 159 (1) (2011) 144–149.
[12] J.N. Huiberts, R. Griessen, J.H. Rector, R.J. Wijngaarden, J.P. Dekker, D.G. de Groot, N.J. Koeman, Nature 380 (1996) 231–234.
[13] T.F. Jaramillo, A. Ivanovskaya, E.W. McFarland, J. Comb. Chem. 4 (2002) 17–22.
[14] M. Pasturel, M. Slaman, H. Schreuders, J.H. Rector, D.M. Borsa, B. Dam, R. Griessen, J. Appl. Phys. 100 (2006) 023515.
[15] B. Farangis, P. Nachimuthu, T.J. Richardson, J.L. Slack, B.K. Meyer, R.C.C. Perera, M.D. Rubin, Solid State Ionics 165 (1–4) (2003) 309–314.
[16] S. Bao, K. Tajima, Y. Yamada, M. Okada, K. Yoshimura, Appl. Phys. A 87 (2007) 621–624.
[17] A. Baldi, D.M. Borsa, H. Schreuders, J.H. Rector, T. Atmakidis, M. Bakker, H.A. Zondag, W.G.J. van Helden, B. Dam, R. Griessen, Int. J. Hydrogen Energy 33 (12) (2008) 3188–3192.
[18] D.M. Borsa, A. Baldi, M. Pasturel, H. Schreuders, B. Dam, R. Griessen, P. Vermeulen, P.H.L. Notten, Appl. Phys. Lett. 88 (2006) 241910.
[19] R. Gremaud, M. Slaman, H. Schreuders, B. Dam, R. Griessen, Appl. Phys. Lett. 91 (2007) 231916.
[20] H. Oguchi, Z. Tan, E.J. Heilweil, L.A. Bendersky, Int. J. Hydrogen Energy 35 (2010) 1296–1299.
[21] J.R. Hattrick-Simpers, K. Wang, L. Cao, C. Chiu, E. Heilweil, R.G. Downing, L.A. Bendersky, J. Alloys Compd. 490 (2010) 42–46.
[22] G. Liang, J. Huot, S. Boily, A. Van Neste, R. Schulz, J. Alloys Compd. 292 (1999).
[23] P. Vermeulen, P. Niessen, P.H.L. Notten, Electrochem. Commun. 8 (1) (2006) 27–32.
[24] P. Vermeulen, R.A.H. Niessen, D.M. Borsa, B. Dam, R. Griessen, P.H.L. Notten, Electrochem. Solid-State Lett. 9 (11) (2006) A520–A523.
[25] A. Sepúlveda, A.F. Lopeandía, R. Domènech-Ferrer, G. Garcia, F. Pi, J. Rodríguez-Viejo, F.J. Muñoz, Int. J. Hydrogen Energy 33 (2008) 2729–2737.
[26] A. Krozer, B. Kasemo, J. Vac. Sci. Technol. A 5 (4) (1987) 1003–1005.
[27] P. Hjort, A. Krozer, B. Kasemo, J. Alloys Compd. 234 (2) (1996) L11–L15.
[28] K. Yoshimura, Y. Yamada, M. Okada, Surf. Sci. 566–568 (2004) 751–754.
[29] J. Qu, Y. Wang, L. Xie, J. Zheng, Y. Liu, X. Li, J. Power Sources 186 (2) (2009) 515–520.
[30] P. Vermeulen, H.J. Wondergem, P.C.J. Graat, D.M. Borsa, H. Schreuders, B. Dam, R. Grissen, P.H.L. Notten, J. Mater. Chem. 18 (2008) 3680–3687.
[31] P. Vermeulen, P.C.J. Graat, H.J. Wondergem, P.H.L. Notten, Int. J. Hydrogen Energy 33 (2008) 5646–5650.
[32] D.M. Borsa, R. Gremaud, A. Baldi, H. Schreuders, J.H. Rector, B. Kooi, P. Vermeulen, P.H.L. Notten, B. Dam, R. Griessen, Phys. Rev. B 75 (2007) 205408.
[33] A. Baldi, R. Gremaud, D.M. Borsa, C.P. Baldi, A.M.J. van der Eerden, G.L. Kruijtzer, P.E. de Jongh, B. Dam, R. Griessen, Int. J. Hydrogen Energy 34 (2009) 1450–1457.
[34] R. Gremaud, A. Baldi, M. Gonzalez-Silveira, B. Dam, R. Griessen, Phys. Rev. B 77 (2008) 144204.